Investigation of lock release gravity currents in an upslope valley

Catherine Jones

October 1, 2013

1 Introduction

The sun heats the land faster than it heats the ocean, causing the air to be warmer over land than over the sea during the day. Convection over land keeps these air masses apart. However, as convection weakens in the afternoon and evening, a pressure gradient causes the cold dense air over the ocean to flow under the warm air on the land in a "sea breeze." In areas where sea breezes occur, they cool the region of land adjacent to the ocean and bring in moisture. In the Santa Barbara region, where valleys penetrate into coastal mountain ranges, sea breezes propagate to high inland plateaus, enabling grapes to be grown; in the absence of sea breezes, the climate would otherwise be too hot and dry. In general, it is of interest to study the flow of dense fluids into valleys and up hills. The results presented here may be applicable not only to coastal agriculture, but also to tidal flows in submarine canyons and estuaries.

Sea breezes are a type of gravity current, and gravity currents are often studied by performing lock-release experiments. This is the approach we take here. A dense fluid is held at one end of the tank by a gate, and the rest of the tank is filled with a lighter fluid. When the gate is removed, the dense fluid, driven by the pressure gradient, flows under the lighter fluid as a gravity current.

The experiments, numerics, and theory in this manuscript explore full-depth lock-release at high Reynolds numbers in the parameter range available when a tank is tilted in the x and y directions, as shown in Figure 1. The aim is to look at the behaviour of gravity currents up slopes and in symmetric and asymmetric V-shaped valleys, and in particular to measure the speed, the time-dependence, and the shape of the currents we observe. We wish to understand what factors control these parameters in order to make general predictions for the initial speed and time dependence of a gravity current in a valley. The timescale of sea breezes is much shorter than one day, and so we do not expect the rotation of the Earth to be important.

In Section 2 of this manuscript we describe previous work on gravity currents, particularly those in valleys and up slopes. In Section 3, we extend Benjamin's analysis to predict the speed and height of a gravity current in a V-shaped valley. A prediction for the speed of upslope flow as a function of slope is also made based on local water depth at the front. In Section 4, we perform laboratory experiments to explore the speed and time dependence

of a gravity current when the tank is tilted in the x and y directions. In Section 5, numerical experiments using the HYbrid Coordinate Ocean Model (HYCOM) are used to shed more light on the experimental results. All of the results are summarised and discussed in Section 6.

2 Background

Lock-release gravity currents with a flat bottom in a rectangular domain are well understood. The initial speed of an energy conserving gravity current, U, is predicted fairly well by Benjamin's analysis, which conserves mass, momentum and energy across the front of the gravity current [1]. It is found that

$$U = \frac{\sqrt{g'H_0}}{2}\,, \tag{1}$$

where H_0 is the height of the fluid at the lock and g' is the reduced gravity for the two fluids. For a flat bottom gravity current, it is understood that there are three phases: the constant speed phase, where the speed of the front is constant, the self-similar phase, where the position of the front X depends on time t as $X(t) \sim t^{\frac{2}{3}}$ and the viscous phase where $X \sim t^{\alpha}$where $\alpha < 1$ and depends on the geometry and set-up [7].

The important parameter for studying the speed of a gravity current is the Froude number, which can be defined in two different ways: one based on the local tank height, H_0 and the other based on h, the height of the gravity current far away from the front:

$$\mathrm{Fr}_H = \frac{U}{\sqrt{g'H_0}}\,, \tag{2a}$$

$$\mathrm{Fr}_h = \frac{U}{\sqrt{g'h}}\,. \tag{2b}$$

Benjamin's analysis predicts that $\mathrm{Fr}_H = \frac{1}{2}$ and $\mathrm{Fr}_h = \sqrt{2}$ for full-depth, flat bottom lock-release.

Downslope gravity currents in rectangular channels are also well understood, both for constant flux down the slope [4] and for a lock release [2]. In both cases, downslope flows have a quasi-constant speed that is a function of slope angle. Experiments show that the nondimensional velocity is maximum at an angle of around 40°. Birman et al. [2] find that for a downslope lock release, Fr_H fits the parabolic curve

$$\mathrm{Fr}_H(\theta < 0) = -0.1924\theta^2 + 0.2781\theta + 0.4871\,, \tag{3}$$

where θ is expressed in radians. This means that for small θ, $\mathrm{Fr}_H(\theta)$ depends approximately linearly on θ. Britter and Linden [4] find that for angles less than 0.5°, downslope flow is no longer quasi-steady, but rather decelerates after the initial constant velocity phase.

Except for a recent study by Ottolenghi et al. [11], upslope gravity currents have received far less attention than downslope gravity currents. Ottolenghi et al. use both experiments and numerics to show that a current decelerates more as the upslope angle increases. They also find that for upslope flow the initial speed of the current does not depend on the slope. Ottolenghi et al. are constrained by the length of their tank, and are only able to achieve

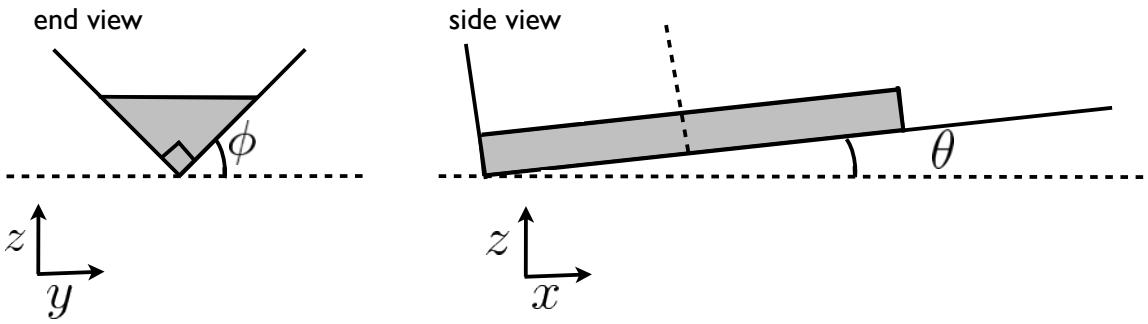

Figure 1: θ and ϕ are the angles that define the orientation of the tank.

slope angles of up to 1.8° in their experiments, and of up to 5° in their numerics. We extend this range to about 8° in both our experiments and our numerics. We also consider upslope flow in V-shaped valleys.

Lock-release flows in symmetric V-shaped valleys have been studied theoretically and experimentally by Monaghan et al. [10] and Marino and Thomas [9]. Monaghan et al. [10] observe that these sorts of currents have a self-similar, parabolic shape and therefore they take a similarity solution approach, assuming a constant value for Fr_h. They predict that the front position X is dependent on time t as $X(t) \sim t^{\frac{4}{5}}$, and they find that their experiments agree with this prediction. Zemach and Ungarish [14] also study flow in a V-shaped valley using shallow water theory, and compare their results to the similarity solution described above. They find good agreement and are able to extend their model to asymmetric basins.

The inital speed of a gravity current in a V-shaped valley has not been predicted analytically in previous work, so we extend Benjamin's analysis for this purpose. We also investigate the effects of tilting a V-shaped valley in the x-z plane, so that the current is flowing up slope. To the best of our knowledge, this experiment has never been done before.

3 Theory

Henceforth, variation in θ is called *rise*, and the variation in ϕ is called *tilt*. These angles are illustrated in Figure 1. They are measured in degrees in the remainder of this manuscript.

3.1 Extension of Benjamin's analysis for $\phi = 45°$

Following Benjamin (1968) [1], we apply conservation of mass, conservation of momentum, and the Bernoulli equation along the free surface and bottom boundary, to find the height and speed of the gravity current. The set-up is shown in Figure 2, in which the frame of reference has been changed so that the front and the dense fluid behind it are stationary. The dense fluid has density ρ_l and the light fluid has density ρ_u. We define the reduced gravity for the two fluids to be

$$g' = \frac{g(\rho_l - \rho_u)}{\rho_u}\,. \tag{4}$$

There are a number of assumptions associated with this approach. It is assumed that gravity waves on the free surface are too fast to affect the speed of the gravity current. It is also assumed that the speed of each layer is relatively uniform, which means that we neglect the effects of viscous boundary layers. Applying Bernoulli along the top and bottom boundaries assumes that there is a streamline along the bottom corner of the tank (at $y = 0$, $z = 0$) and along the free surface (at $y = H$, $z = 0$). This is justified by symmetry considerations in the $\phi = 45°$ case. It is also assumed that energy is conserved along these lines, which is not strictly true, but a good approximation.

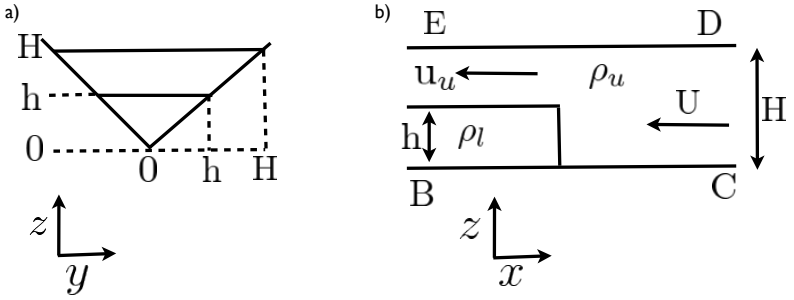

Figure 2: Schematic of the $\phi = 45^0$, $\theta = 0^0$ setup. a) shows a cross section view at BE and b) shows a section along the tank at $y = 0$.

The mass flowing through the cross section at BE must equal the mass flowing through the cross section at DC, so

$$H^2 U = \left(H^2 - h^2\right) u_u \,. \tag{5}$$

Then applying Bernoulli along BC and ED gives

$$p_B = p_C + \frac{\rho_u U^2}{2} \,, \tag{6a}$$

$$p_E + \frac{\rho_u u_u^2}{2} = p_D + \frac{\rho_u U^2}{2} \,. \tag{6b}$$

Integrating the hydrostatic equation, $\frac{dp}{dz} = -\rho g$, we find that the pressure in the cross-section at BE is

$$p = \begin{cases} p_B - \rho_l g z & \text{if } z < h; \\ p_B - \rho_l g h - \rho_u g \left(z - h\right) & \text{if } z > h. \end{cases} \tag{7}$$

and the pressure in the cross-section at CD is

$$p = p_C - \rho_u g z. \tag{8}$$

Now we conserve the flux of momentum through the tank. The flux of momentum through the cross section at BE must be equal to the flux of momentum through the cross section at CD. We consider only the positive half of the domain, because symmetry dictates that

flow in the negative half behaves identically. Conserving momentum,

$$\int_0^h \int_y^h p_B - \rho_l g z \,\mathrm{d}z\mathrm{d}y + \int_0^h \int_h^H p_B - \rho_l g h - \rho_u g\,(z-h) + \rho_u u_u^2 \,\mathrm{d}z\mathrm{d}y + \int_h^H \int_y^H p_B - \rho_l g h - \rho_u g\,(z-h) + \rho_u u_u^2 \,\mathrm{d}z\mathrm{d}y = \int_0^H \int_y^H p_C - \rho_u g z + \rho_u U^2 \mathrm{d}z\mathrm{d}y\,. \tag{9}$$

Integrating with respect to z yields

$$\begin{aligned}\int_0^h p_B\,(h-y) - \rho_l g\left(\frac{h^2}{2} - \frac{y^2}{2}\right)\,\mathrm{d}y \\ + \int_0^h \left(p_B - \rho_l g h + \rho_u g h + \rho_u u_u^2\right)(H-h) - \rho_u g\left(\frac{H^2}{2} - \frac{h^2}{2}\right)\mathrm{d}y \\ + \int_h^H \left(p_B - \rho_l g h + \rho_u g h + \rho_u u_u^2\right)(H-y) - \rho_u g\left(\frac{H^2}{2} - \frac{y^2}{2}\right)\mathrm{d}y \\ = \int_0^H p_C\,(H-y) - \rho_u g\left(\frac{H^2}{2} - \frac{y^2}{2}\right) + \rho_u U^2\,(H-y)\,\mathrm{d}y\,.\end{aligned} \tag{10}$$

Rearranging, and then integrating with respect to y gives

$$\begin{aligned}&\left(p_B - \rho_l g h + \rho_u g h + \rho_u u_u^2\right)\left(\frac{H^2}{2} - \frac{h^2}{2}\right) \\ &+ p_B\left(h^2 - \frac{h^2}{2}\right) - \rho_l g\left(\frac{h^3}{2} - \frac{h^3}{6}\right) + \frac{\rho_u g}{2}\left(h^3 - H^3\right) + \rho_u g\left(\frac{H^3}{6} - \frac{h^3}{6}\right) \\ &= p_C\left(H^2 - \frac{H^2}{2}\right) - \rho_u g\left(\frac{H^3}{2} - \frac{H^3}{6}\right) + \rho_u U^2\left(H^2 - \frac{H^2}{2}\right).\end{aligned} \tag{11}$$

Then substituting in for p_C using equation Eq. (6a), and expressing $g(\rho_l - \rho_u)/\rho_u$ as g',

$$g'\frac{h^3}{6} - g' h \frac{H^2}{2} + U^2\frac{H^2}{4} + u_u^2\left(\frac{H^2}{2} - \frac{h^2}{2}\right) = U^2\frac{H^2}{2}\,. \tag{12}$$

into which we can substitute for u_u using Eq. (5), giving

$$g'\frac{h^3}{6} - g' h \frac{H^2}{2} = \frac{U^2 H^2}{2}\left(\frac{1}{2} - \frac{H^2}{(H^2 - h^2)}\right). \tag{13}$$

Again using the hydrostatic equation, the pressures at B, C, D and E are related by

$$p_E = p_B - \rho_l g h - \rho_u g\,(H-h) \tag{14a}$$

$$p_D = p_C - \rho_u g H\,. \tag{14b}$$

Using the above expression and Eq. (6a), Eq. (6b) can be rewritten as

$$\frac{u_u^2}{2} = g' h\,. \tag{15}$$

Applying mass conservation (Eq. (5)),

$$\frac{\left(H^2-h^2\right)^2 g'h}{H^2} = \frac{H^2U^2}{2}\,, \tag{16}$$

which relates the speed of the current U to its height h. We can substitute Eq. (16) into Eq. (13) to give an expression for the height of the current h in terms of the total height of the tank H,

$$h^2 = \frac{H^2}{3}\,. \tag{17}$$

This means that in a symmetric V-shaped valley, the height of the gravity current is $H/\sqrt{3}$, which is taller than $H/2$, the height of a gravity current in a rectangular channel. We can obtain the speed of the current by substituting Eq. (17) back into Eq. (16) and rearranging, giving

$$U^2 = 2g'\left(\frac{2}{3}\right)^2\sqrt{\frac{1}{3}}H\,. \tag{18}$$

Therefore the predicted Froude number for a V-shaped valley with $\phi = 45^\circ$ is

$$\begin{aligned}\mathrm{Fr}_H(\phi=45^\circ) = \frac{U}{\sqrt{g'H}} &= \sqrt{\frac{8}{9\sqrt{3}}} \\ &\approx 0.72\,.\end{aligned} \tag{19}$$

This is significantly larger than the prediction $\mathrm{Fr}_H(\phi = 0^\circ) = \frac{1}{2}$ for a gravity current in a rectangular channel. Qualitatively, this result can be explained using conservation of mass. Because the tank is wider at the top in the valley case, the gravity current can be taller than $H/2$ without restricting the return flow, which has a speed $u_u - U$. A taller gravity current is usually associated with a faster front speed, because it leads to a higher difference in pressure at the front. Even though the front is taller in the $\phi = 45^\circ$ case, the return flow is still slower than the gravity current.

3.2 Extension of Benjamin's analysis for general ϕ

Here we extend the Benjamin's analysis above for general ϕ. A schematic of the set-up is shown in Fig. 3. Again, conservation of mass gives

$$H^2U = \left(H^2-h^2\right)u_u\,. \tag{20}$$

We then apply Bernoulli along BC and ED. It is important to note that applying Bernoulli at the corner of the tank is a very strong assumption. A streamline along the bottom corner of the tank may not exist, because the valley is no longer symmetric. Bernoulli yields

$$p_B = p_C + \frac{\rho_u U^2}{2}\,, \tag{21a}$$

$$p_E + \frac{\rho_u u_u^2}{2} = p_D + \frac{\rho_u U^2}{2}\,. \tag{21b}$$

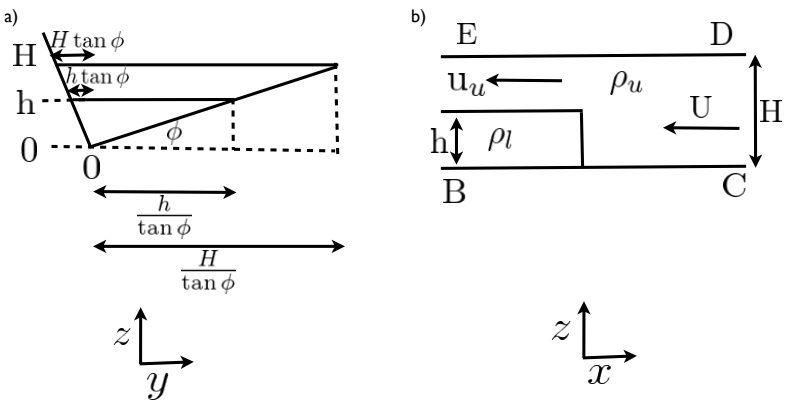

Figure 3: Schematic of the $\theta = 0$ setup for general ϕ. a) shows a cross section view at BE and b) shows a section along the tank at $y = 0$.

Integrating the hydrostatic equation, $\frac{dp}{dz} = -\rho g$, we find that the pressure in the cross-section at BE is

$$p = \begin{cases} p_B - \rho_l g z & \text{if } z < h; \\ p_B - \rho_l g h - \rho_u g\,(z-h) & \text{if } z > h. \end{cases} \tag{22}$$

and the pressure in the cross-section at DC is

$$p = p_C - \rho_u g z. \tag{23}$$

Now we conserve momentum flux, which can be expressed as a sum of the flux of momentum in the positive section of the domain and the flux of momentum in the negative section of the domain,

$$\sum_{i=1,2}\left(\int_0^{\mu_i h}\int_{y/\mu_i}^{h} p_B - \rho_l g z\,\mathrm{d}z\mathrm{d}y + \int_0^{\mu_i h}\int_h^H p_B - \rho_l g h - \rho_u g\,(z-h) + \rho_u u_u^2\,\mathrm{d}z\mathrm{d}y + \right.$$
$$\left.\int_{\mu_i h}^{\mu_i H}\int_{y/\mu_i}^{H} p_B - \rho_l g h - \rho_u g\,(z-h) + \rho_u u_u^2\,\mathrm{d}z\mathrm{d}y = \int_0^{\mu_i H}\int_{y/\mu_i}^{H} p_C - \rho_u g z + \rho_u U^2 \mathrm{d}z\mathrm{d}y\right), \tag{24}$$

where $\mu_1 = \tan\phi$ and $\mu_2 = 1/\tan\phi$. In what follows, the summation is implied by the subscript i. We integrate with respect to z first to give

$$\int_0^{\mu_i h} p_B\left(h - \frac{y}{\mu_i}\right) - \rho_l g\left(\frac{h^2}{2} - \frac{y^2}{2\mu_i^2}\right)\mathrm{d}y$$
$$+ \int_0^{\mu_i h}\left(p_B - \rho_l g h + \rho_u g h + \rho_u u_u^2\right)(H-h) - \rho_u g\left(\frac{H^2}{2} - \frac{h^2}{2}\right)\mathrm{d}y$$
$$+ \int_{\mu_i h}^{\mu_i H}\left(p_B - \rho_l g h + \rho_u g h + \rho_u u_u^2\right)\left(H - \frac{y}{\mu_i}\right) - \rho_u g\left(\frac{H^2}{2} - \frac{y^2}{2\mu_i^2}\right)\mathrm{d}y$$
$$= \int_0^{\mu_i H} p_C\left(H - \frac{y}{\mu_i}\right) - \rho_u g\left(\frac{H^2}{2} - \frac{y^2}{2\mu_i^2}\right) + \rho_u U^2\left(H - \frac{y}{\mu_i}\right)\mathrm{d}y\,. \tag{25}$$

We then integrate with respect to y to give

$$\begin{aligned}
&p_B\left(\mu_i h^2 - \frac{\mu_i h^2}{2}\right) - \rho_l g\left(\frac{\mu_i h^3}{2} - \frac{\mu_i h^3}{6}\right) + \mu_i h\left(p_B - \rho_l g h + \rho_u g h + \rho_u u_u^2\right)(H-h) \\
&- \mu_i h \rho_u g\left(\frac{H^2}{2} - \frac{h^2}{2}\right) + \left(p_B - \rho_l g h + \rho_u g h + \rho_u u_u^2\right)\left(\mu_i H^2 - \mu_i h H - \frac{\mu_i H^2}{2} + \frac{\mu_i h^2}{2}\right) \\
&- \rho_u g\left(\frac{\mu_i H^3}{2} - \frac{\mu_i H^2 h}{2} - \frac{\mu_i H^3}{6} + \frac{\mu_i h^3}{6}\right) \\
&= p_C\left(\mu_i H^2 - \frac{\mu_i H^2}{2}\right) - \rho_u g\left(\frac{\mu_i H^3}{2} - \frac{\mu_i H^3}{6}\right) + \rho_u U^2\left(\mu_i H^2 - \frac{\mu_i H^2}{2}\right).
\end{aligned} \tag{26}$$

At this point, we can divide through by μ_i to give Eq. 11, meaning that the predictions of Benjamin's theory in an asymmetric valley are the same as those in a symmetric valley, i.e.

$$h^2 = \frac{H^2}{3}. \tag{27}$$

and

$$\begin{aligned}
\mathrm{Fr}_H(\phi) = \frac{U}{\sqrt{g'H}} &= \sqrt{\frac{8}{9\sqrt{3}}} \\
&\approx 0.72.
\end{aligned} \tag{28}$$

Surprisingly, the results are independent of ϕ. It seems likely that this does not reflect the effects of changing ϕ in the real world, and is instead a consequence of the strong assumption that there is a streamline along the bottom corner of the tank. In the symmetric ($\phi = 45°$) case, the streamline must follow the bottom corner of the tank, because the flow must be symmetric (this assertion will be validated by the laboratory experiments). However, in the asymmetric case, it is unlikely that a streamline exists along the bottom corner, because flow down the walls will occur at different speeds. It is possible that a streamline exists somewher on the wall, and this may be something we investigate in future. That $\mathrm{Fr}_H(\phi)$ does not approach $\frac{1}{2}$ as $\phi \to 0°$ may reflect the importance of having both left and right boundaries in a channel flow.

3.3 Prediction of deceleration in the upslope, no tilt case.

One way to predict the deceleration of upslope flow on a flat bottom is to assume a constant Froude number, Fr_H, and therefore assume that the speed of the current is only dependent on local water depth at the front. First we express the speed of the current U in terms of the Froude number, reduced gravity and local water depth, which is a function of distance along the tank.

$$U = \mathrm{Fr}\sqrt{g'H(x)}. \tag{29}$$

If $s = \tan\theta$ is the slope and H_0 is the height of the water at the lock, U can be expressed in terms of the distance of the front from the lock x to give

$$U = \mathrm{Fr}\sqrt{g'H_0}\sqrt{1 - \frac{sx}{H_0}}. \tag{30}$$

Defining $U_0 = \mathrm{Fr}\sqrt{g'H_0}$ yields the differential equation

$$\frac{dx}{dt} = U_0\sqrt{1 - \frac{sx}{H_0}}\,. \tag{31}$$

When we solve this differential equation, we get

$$X = x_0 + U_0 t - \frac{U_0^2 t^2 s}{4H_0}\,. \tag{32}$$

This result was separately derived in the study of shoaling surface gravity currents passing over an underlying slope [8]. For large values of H_0 or small values of s, we expect that the effect of the local water depth will no longer dominate, and other effects like energy conservation will become important. However, for the shallow water in our experiments, the effect of water depth may dominate over these other effects.

4 Laboratory experiments

We first explore the validity of the extended Benjamin results and the predictions for upslope flow by comparing them to the results of laboratory experiments. The experiments explore the parameter range shown in Table 1, where θ and ϕ are defined as in Figure 1.

The tank is 148cm long, 19.8cm wide and 28.7cm tall, and the lock is 36.7cm long, occupying approximately a quarter of the total volume of the tank. The short length of the tank allows us to explore a larger range of θ than in previous studies [11]. For the majority of experiments the tilt is either $\phi = 0^\circ$ or $\phi = 45^\circ$, although $\phi = 15^\circ$ and $\phi = 30^\circ$ cases are also considered.

The density of the fluid in the lock is increased by adding salt, and colored food dye is also added in order to make the current visible. The reduced gravity g' for each experiment is around 6 cm/s^2, although it varies slightly due to inaccuracies in measuring the volume of the tank and the amount of salt added. This should not affect the results, which are nondimensionalized using the particular value of g' for each experiment.

The experiments are recorded in black and white so that the shape and location of the front can be tracked. The camera position varies with experiment (see Figure 4), and a mirror is placed at 45° to the side of the tank in order to give another view of the current. In the $\phi = 0^\circ$ case the mirror shows the shape of the front, and the top view shows the amount of three-dimensionality in the current. In the $\phi \neq 0^\circ$ cases, the mirror allows us to see how symmetric the current is and to check that the top edge of the tank does not obstruct too much of the current.

In the case where $\phi = 0^\circ$ the current is approximately two-dimensional, but a small amount of three-dimensionality occurs due to instabilities and asymmetry in the removal of the gate. In order to quantify the error due to three-dimensional instabilies, three time series of the current are taken at five centimeter intervals across the tank (shown in Figure 5).

One of these time series with $\theta = 6.2^\circ$ is shown in Figure 6. A threshold brightness is chosen to define the front, and a series of points is generated giving the position of the front in each frame. Points are not taken in the first few seconds after the gate is pulled, because there is a short period of readjustment when the gate is removed and the location of the

$\phi(^\circ)$	$\theta(^\circ)$	g' (m/s^2)
0	0	6.6
0	1	6.6
0	1.9	6.4
0	2.9	6.1
0	3.9	6.7
0	4.8	6.8
0	6.2	6.2
0	7.0	6.7
0	8.1	7.4
45	0	5.9
45	0.9	6.0
45	1.9	5.3
45	2.9	6.6
45	3.8	6.2
45	5.2	6.1
45	6.2	6.2
45	6.6	6.3
45	8.0	6.7
15	0	6.7
15	6.2	6.1
30	0	6.2
30	6.2	6.5

Table 1: The parameter range of the experiments.

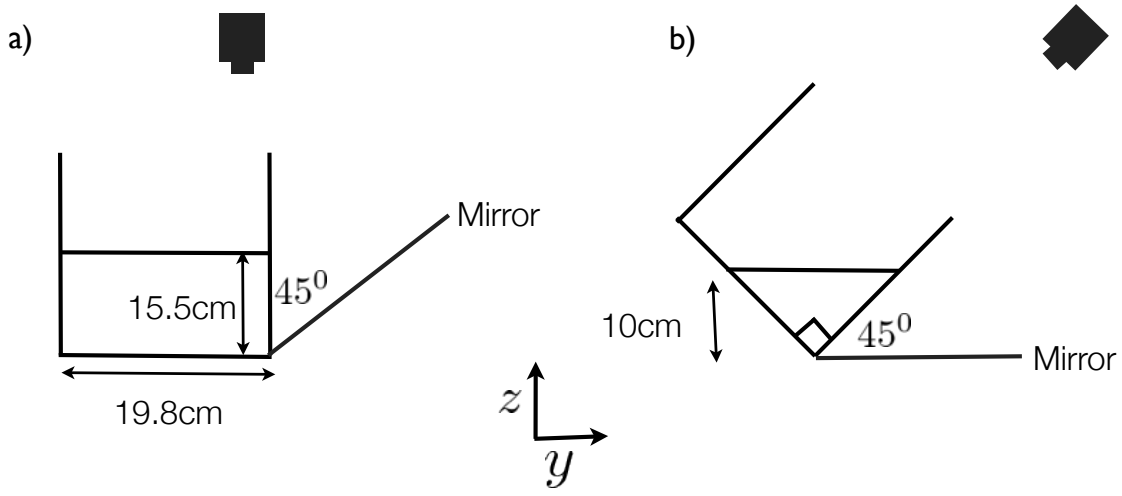

Figure 4: The location of the camera with respect to the tank when a) $\phi = 0°$, and b) $\phi = 45°$.

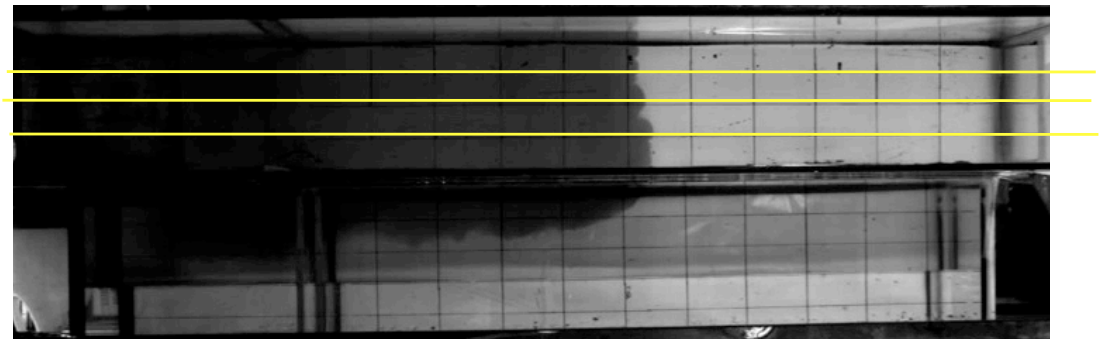

Figure 5: When $\phi = 0°$, three time series are taken at 5cm intervals across the tank.

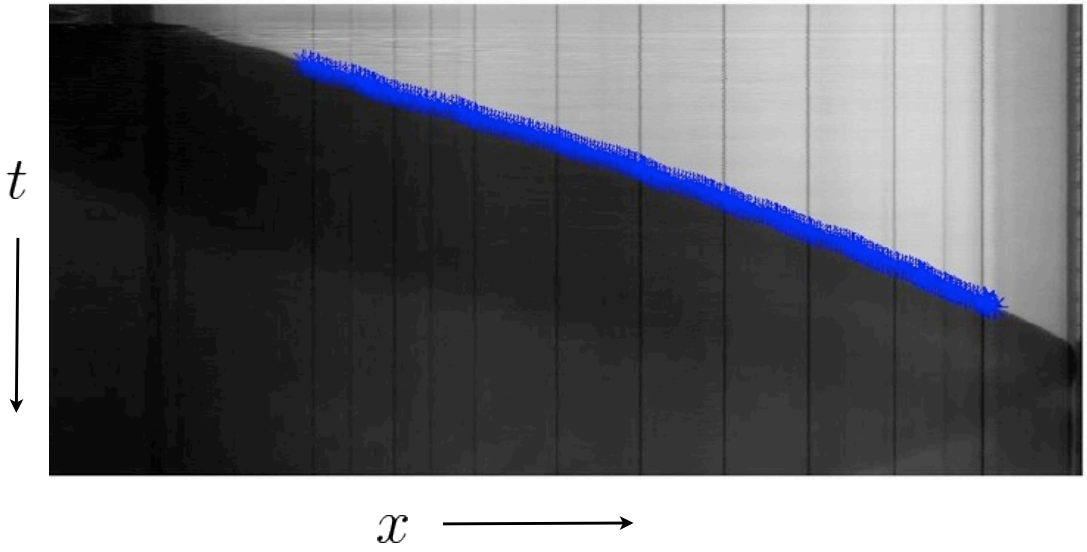

Figure 6: Time series taken when $\theta = 6.2°$ (black and white image) and points showing the loaction of the front away from the initial readjustment.

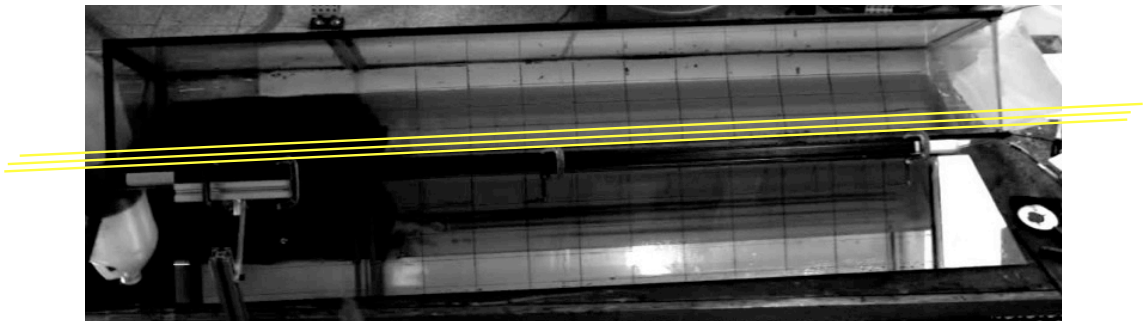

Figure 7: When $\phi = 45°$, ten time series are taken at 1 pixel intervals starting at the tank edge and moving upward.

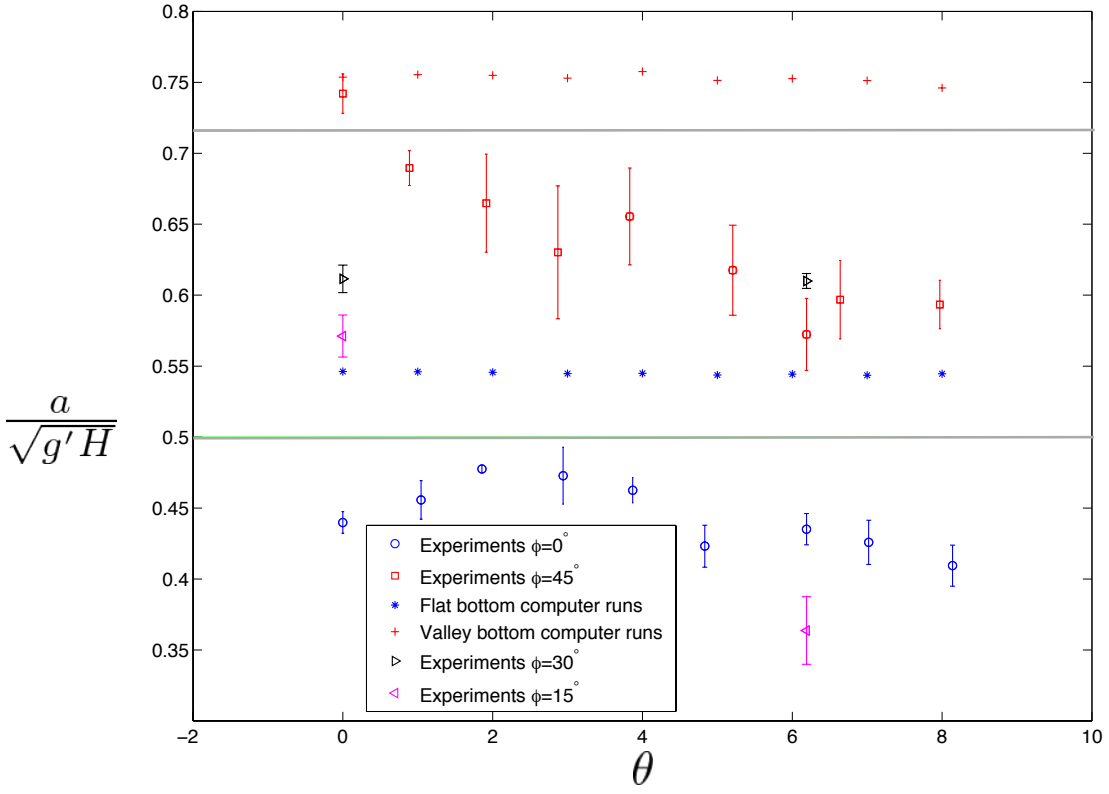

Figure 8: Initial gravity current speed a for the experimental data and numerical simulations, when front position is fitted with the line $X(t) = x_0 + at + bt^2$. The grey lines indicate the theoretical results.

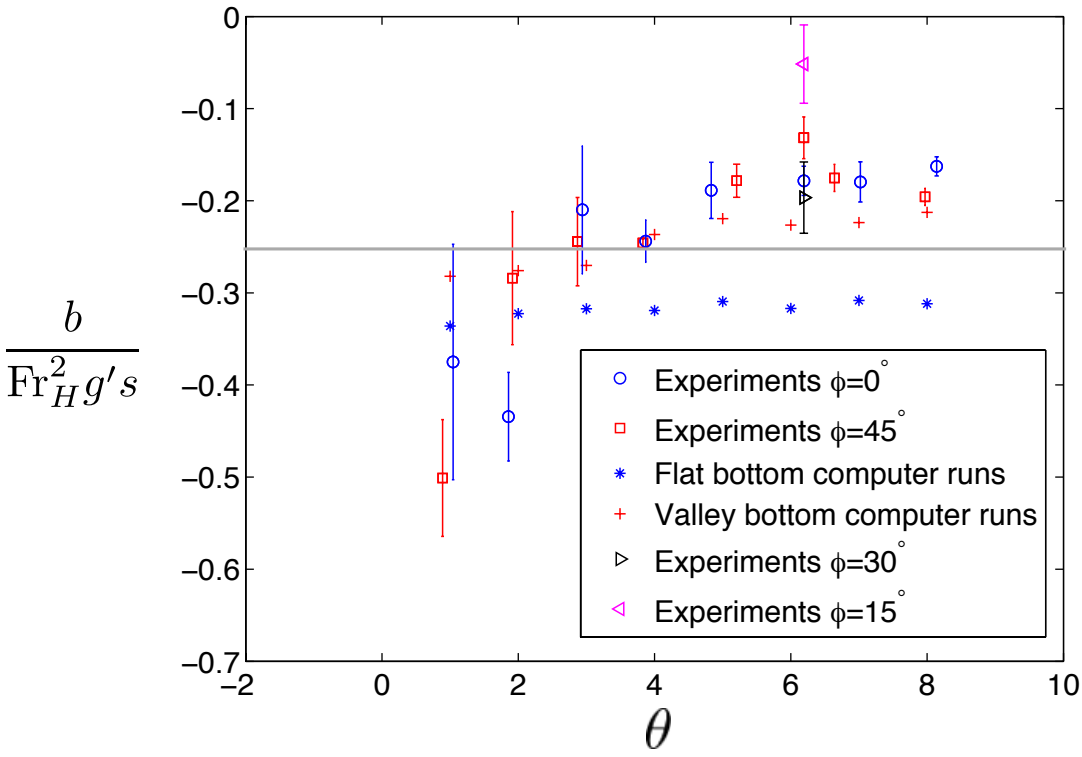

Figure 9: Relative double-acceleration, b for the experimental data and numerical simulations, normalized using $U_0 = \mathrm{Fr}_H\sqrt{g'H_0}$, where Fr_H from the $\theta = 0°$ case is taken as a prediction of Fr_H for all θ when front position is fitted with the line $X(t) = x_0 + at + bt^2$. The grey line indicates the theoretical result.

front is unclear because of the turbulence generated. However, the time at which the gate is pulled is recorded as $t = 0$. Because the theory predicts that $x = x_0 + U_0 t - \frac{U_0^2 t^2 s}{4H_0}$, a quadratic of the form $X(t) = x_0 + at + bt^2$ is fitted to the points for each of the three time series, and then the mean values of a and b are taken. Error bars are generated based on the spread of the three values.

In the case where $\phi \neq 0°$, the current is three-dimensional, and the main source of error is that the time series is not taken in the fastest part of the current (which is at the corner of the tank). In order to mitigate for this, ten time series are taken, starting at the edge of the tank and moving upwards by one pixel for each new time series (see Figure 7). The clearest three to five are used. This is necessary because some of the lines chosen overlap with the edge of the tank, while others are too far from the center line and therefore do not exhibit a well-defined front due to turbulence.

The results of the laboratory experiments are shown in Figures 8, 9 and 10. In all cases $X(t) = x_0 + at + bt^2$ is a good fit to the data. It is likely that the error bars on a and b for $\phi = 45°$ are too small, probably because the lines chosen for time series are not completely parallel to the centerline of the current. If a time series is taken at an angle to the centerline

of the current, both the initial speed a and the relative double-acceleration b are likely to be too small.

In the $\phi = 0°$ case, $\mathrm{Fr}_H(t=0) = \frac{a}{\sqrt{g'H_0}}$ is 10 to 20% less than the predicted value of 0.5. This is typical for the results of lock exchange experiment [13], and is probably because energy conservation is an approximation. While the Benjamin result strictly only applies in the $\theta = 0°$ case, there is no reason why the initial speed should change when $\theta \neq 0°$, and the results show that a remains relatively constant with changing θ. This is consistent with the results of Ottolenghi et al. [11], who also found that the initial speed does not change with rise for a gravity current in a rectangular channel.

In the $\phi = 45°$ case, the inital speed a decreases with increasing rise θ. This is a surprise, and is not yet understood. We hypothesize that the initial velocity of the front in the upslope case is slowed by turbulent momentum transport from the sides of the valley. The flow at the sides of the valley is slower than the flow in the middle, and so any momentum transport from there would cause a slowing of the gravity current.

The normalized deceleration $\frac{b}{\mathrm{Fr}_H g' s}$ is plotted in Figure 9. Given that we expect that $X(t) = x_0 + U_0 t - \frac{U_0^2 t^2 s}{4H_0}$, if a were independent of rise and $U_0 = \mathrm{Fr}_H\sqrt{g'H_0}$ where Fr_H is predicted by the theory for the zero slope case, then

$$\frac{b}{Fr_H^2 g' s} = \frac{1}{4}\,. \tag{33}$$

The data does not fit Eq. (33) very well because a does not fit the theoretical result very well. If we do not assume that Benjamin theory and its extension holds, we expect that

$$\frac{bH_0}{a^2 s} = \frac{1}{4}\,. \tag{34}$$

The data fits Eq. (34) except at small angles, where s is small, causing errors to be magnified (see Figure 10). It is also possible that for small rise, other effects are important for decelerating the flow, for example, energy conservation or viscosity. In fact, it is surprising that our predictions hold so well for the majority of the angles studied.

For the asymmetric valley cases, the results do not agree well with Benjamin's analysis. This is probably because the assumption of a streamline along the bottom of the domain is incorrect. In particular, the case $\theta = 6.2°$, $\phi = 15°$ is very far from the expected value for $\mathrm{Fr}_H(\phi = 15°) = \frac{a}{\sqrt{g'H}}$ of 0.72. However, in these cases b still fits well with Eq. 34, suggesting that the dependence of deceleration on changing water depth still holds. More experiments are needed in order to say anything further about the effects of asymmetry.

5 Numerical experiments

The HYbrid Coordinate Ocean Model (HYCOM) [3], [5], [6] is a hydrostatic model that solves the shallow water equations. We use a two layer set up in the same geometry as the experiments, and with a grid spacing of 0.5cm. g' is approximately the same as the experiments, but the computational Reynolds number is 1200, lower than the experimental Reynolds number of 7000. Varying viscosity does not produce major changes in the model output, so the difference in Reynolds number is not likely to affect the results very

Parameter	Descripton	Value
visco2	deformation-dependent Laplacian viscosity factor	0.05
visco4	deformation-dependent biharmonic viscosity factor	0
veldf2	diffusion velocity (m/s) for Laplacian momentum dissipation	0.01
veldf4	diffusion velocity (m/s) for biharmonic momentum dissipation	0.01
thkdf2	diffusion velocity (m/s) for Laplacian thickness diffusion	0.001
thkdf4	diffusion velocity (m/s) for biharmonic thickness diffusion	0

Table 2: Parameters for diffusion of momentum in the HYCOM model. These parameters aim to compensate for the lack of turbulence in the model. However, our results are fairly robust and small changes to these parameters do not affect the speed and time dependence of the current (though they do change the shape of the front).

much. Further parameters used in HYCOM are shown in Table 2. These parameters were tuned until the shape of the front resembled the laboratory experiments. Changes in these parameters do not affect a and b noticably.

In the numerical model, the front is defined as the first location at which the bottom layer is thicker than 0.5cm. As in the laboratory, $X(t) = x_0 + at + bt^2$ is fitted to a time series of front position.

Figure 11 shows a comparison between the shape of the gravity current in the model and in the laboratory. Away from the front, the height of the current is similar in both cases, but shape of the head of the current in the model is very different from the shape of the head of the current in the experiment. This difference is probably because the model is hydrostatic and the processes at the front are non-hydrostatic. Benjamin analysis requires the assumption that the height of the current tends to a constant value far away from the front. We can see from Figure 11 that this is a valid assumption.

In the numerical simulation, there are a lot more waves at the interface in the valley case than in zero tilt case. The experiments are also a little more irregular, consistent with observations by Monaghan et al. [10]. This might perhaps be due to the two speeds involved in the valley case: the speed of the current along the tank (in the x-direction) and the speed at which the fluid collapses into the middle of the tank (in the y-direction). The irregularity may be more pronounced in the model because it does not allow turbulence so the waves cannot dissipate their energy so easily.

HYCOM allows us to look at the cross-section of the current, something that is difficult to do in the laboratory experiment. In cross-section it is observed that far away from the front, the interface is flat, as one would expect, but near to the front the height of the interface varies in the y-direction, and the center of the current is higher than the edges.

Figures 8, 9 and 10 show the results of both the numerical simulations and laboratory experiments. In the numerical experiments, $\mathrm{Fr}_H(t=0) = \frac{a}{\sqrt{g'H_0}}$ is higher than the predictions of Benjamin's analysis and its extension. This is unsurprising because in the model, Bernoulli does not necessarily apply along the top and bottom boundaries and because the model is hydrostatic, it does not conserve momentum exactly. Faster speeds are often available when this sort of condition is relaxed [12].

In the HYCOM model, the initial speed a is independent of θ. It is hypothesized

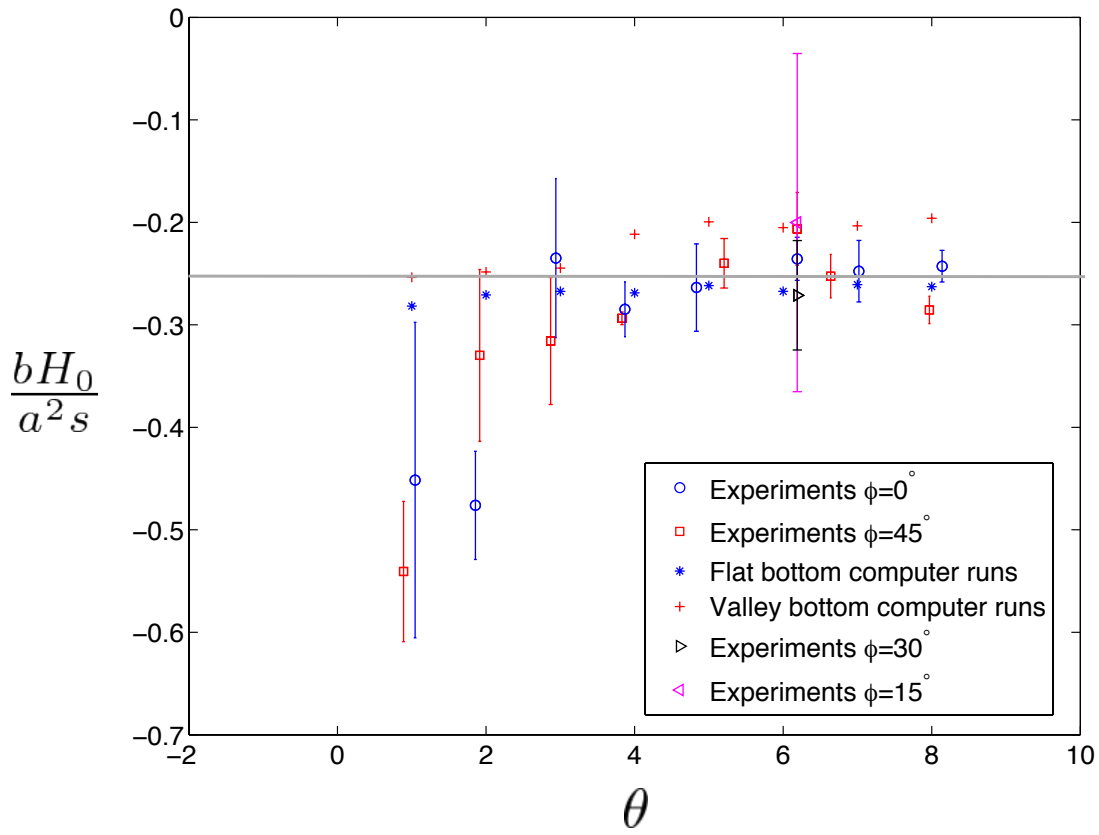

Figure 10: Relative double-acceleration b for the experimental data and numerical simulations, normalized using the measured initial speed a when front position is fitted with the line $X(t) = x_0 + at + bt^2$. The grey line indicates the theoretical results.

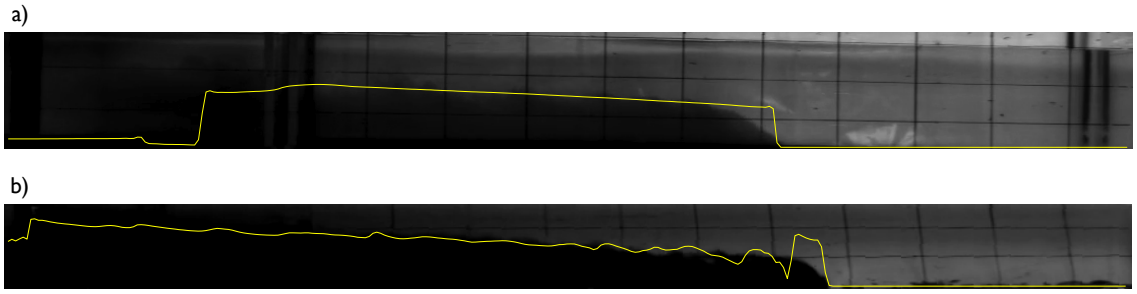

Figure 11: Comparison of head shape between the numerical model (yellow line) and the experiments for the case a) $\phi = 0°$, $\theta = 0°$ and b) $\phi = 45°$, $\theta = 0°$.

that turbulent momentum transport from the sides of the valley is responsible for the slower current in the laboratory. This fits well with the numerical results because turbulent momentum transport does not occur in the HYCOM model, so it is expected that a should be independent of θ in the model.

6 Summary and Discussion

Theory, experiments and numerics agree that a gravity current in a valley is faster than a gravity current in a rectangular channel, and specifically that $\mathrm{Fr}_H = 0.72$ for a symmetric valley where $\phi = 45°$. While theory, experiments and numerics differ slightly, this is not unexpected, because the theory makes assumptions about conservation of energy that are not necessarily followed in the experiments or numerics.

Laboratory experiments show that, unlike in the $\phi = 0°$ case, the initial speed of the gravity current in the $\phi = 45°$ case decreases as θ increases and it is unclear what causes this. However, we hypothesize that lateral turbulent momentum transport moves momentum away from the fast moving center of the current into the slower moving edges where the depth is much shallower.

To first order, the upslope flow speed seems to be controlled by the local depth of the fluid in the parameter range explored here. Gravitational acceleration, bottom drag, and viscosity are secondary effects, and the role of these need further investigation, since in currents with bigger H_0, smaller s or smaller g', the role of these effects will probably be larger. This is likely to be the case in real-world applications like sea breezes up valleys, where H_0 is not clearly defined. For small slopes, the predictions based on local fluid depth do not fit the data well, and this is likely to be because some of these other effects are important.

In an attempt to compare our results with Monaghan et al. [10]'s prediction for the time dependence of front position, a fit to a log-log plot of the front position in the zero slope cases of both the laboratory and numerical experiments was taken. However, in both cases it was found that front position $X \sim t$ rather than $X \sim t^{\frac{4}{5}}$. It may be that the time series taken in our experiments and numerics was not long enough. Monaghan et al. used a tank that was more than fifteen lock lengths long, whereas our tank was only about four lock lengths long. It is also possible that the assumption of self-similarity in Monaghan et al.'s theory is invalid in our flow, but this seems unlikely since the current has the same self-similar shape as Monaghan et al. describe.

More investigation is needed into why the initial speed predicted by the model differs from the initial speed measured in the laboratory. This could be done by simulating the flow in a Direct Numerical Simulation that includes lateral momentum transfer via turbulence. Alternatively, an experiment in which the viscosity of the flow was increased (so that turbulence was surpressed) could be performed, though this would introduce viscous boundary layer effects.

There are still many questions to be answered in understanding how topography steers gravity currents. It would be interesting to look at the effect of changing the angle inside the valley, since the sides of most valleys in the real world slope less than those in my experiment. We would also like to look at the transfer between kinetic and potential energy

in the numerical model, because it is surprising that this does not appear to play a role in the upslope speed of a gravity current.

7 Acknowledgements

I would like to thank my advisors, Eric Chassignet, Bruce Sutherland, Claudia Cenedese and Paul Linden. I would also like to thank Flavien Gouillon and Alexandra Bozec for their help in setting up the HYCOM model.

References

[1] T. B. Benjamin, *Gravity currents and related phenomena*, J. Fluid Mech., 31 (1968), pp. 209 – 248.

[2] V.K. Birman, E. Meiburg, and M. Ungarish, *On gravity currents in stratified ambients*, Phys. Fluids., 19 (2007).

[3] R Bleck, *An oceanic general circulation model framed in hybrid isopycnic? cartesian coordinates.*, Ocean Modeling, 4 (2002), pp. 55–88.

[4] R. E. Britter and P. F. Linden, *The motion of the front of a gravity current travelling down an incline*, J. Fluid Mech., 99 (1980), pp. 531–543.

[5] E.P. Chassignet, LT Smith, GR Halliwell, and R Bleck, *North atlantic simulations with the hybrid coordinate ocean model (hycom): Impact of the vertical coordinate choice, reference density, and thermobaricity*, J. Phys Oceanogr., 33 (2003), pp. 2504–2526.

[6] GR Halliwell, *Evaluation of vertical coordinate and vertical mixing algorithms in the hybrid-coordinate ocean model (hycom)*, Ocean Modeling, 7 (2004), pp. 285–322.

[7] H.E. Huppert, *The propagation of two-dimensional and axisymmetric viscous gravity currents over a rigid horizontal surface*, J. Fluid Mech., 121 (1982), pp. 43–58.

[8] G. H. Keulegan, *The motion of saline fronts in still water*, Natl Bur. Stnd. Rep., 5813 (1958).

[9] B. M. Marino and L. P. Thomas, *Dam-break release of a gravity current in a power-law channel section*, J. Phys.: Conf. Ser., 296 (2011), pp. 1–10.

[10] J.J. Monaghan, C.A. Meriaux, H.E. Huppert, and J.M. Monaghan, *High reynolds number gravity currents along v-shaped valleys*, European Journal of Mechanics - B/Fluids, 28 (2009), pp. 651 – 659.

[11] L. Ottolenghi, C. Adduce, V. Armenio, R. Inghilesi, and F. Roman, *Large eddy simulation of lock-exchange gravity currents moving on upsloping beds.* Unpublished manuscript.

[12] J. O. Shin, S. B. Dalziel, and P. F. Linden, *Gravity currents produced by lock exchange*, J. Fluid Mech., 521 (2004), pp. 1–34.

[13] B.R. Sutherland, D Polet, and M. Campbell, *Gravity currents shoaling on a slope*, Phys. Fluids., 25 (2013).

[14] T Zemach and M Ungarish, *Gravity currents in non-rectangular cross-section channels: Analytical and numerical solutions of the one-layer shallow-water model for high-reynolds-number propagation*, Physics of Fluids, 5 (2012), p. 026601.